Robust Single-Image Super-Resolution Based on Adaptive Edge-Preserving Smoothing Regularization

Shuying Huang, Member, IEEE, Jun Sun, Yong Yang[®], Senior Member, IEEE, Yuming Fang, Member, IEEE, Pan Lin, Member, IEEE, and Yue Que

Abstract—Single-image super-resolution (SR) reconstruction via sparse representation has recently attracted broad interest. It is known that a low-resolution (LR) image is susceptible to noise or blur due to the degradation of the observed image, which would lead to a poor SR performance. In this paper, we propose a novel robust edge-preserving smoothing SR (REPS-SR) method in the framework of sparse representation. An EPS regularization term is designed based on gradient-domain-guided filtering to preserve image edges and reduce noise in the reconstructed image. Furthermore, a smoothing-aware factor adaptively determined by the estimation of the noise level of LR images without manual interference is presented to obtain an optimal balance between the data fidelity term and the proposed EPS regularization term. An iterative shrinkage algorithm is used to obtain the SR image results for LR images. The proposed adaptive smoothing-aware scheme makes our method robust to different levels of noise. Experimental results indicate that the proposed method can preserve image edges and reduce noise and outperforms the current state-of-the-art methods for noisy

Index Terms—Single image super-resolution, guided image filtering, regularization, edge preserving.

I. INTRODUCTION

IGH-RESOLUTION (HR) images play an important role in many image applications, such as remote sensing, medical diagnosis, surveillance video and pattern recognition [1], [2]. However, due to the limitations of image acquisition and storage devices in some real applications, the image resolution cannot satisfy practical demand [3]. To increase image resolution, one direct solution is to reduce the pixel

Manuscript received August 28, 2017; revised January 13, 2018; accepted February 18, 2018. Date of publication February 27, 2018; date of current version March 12, 2018. This work was supported in part by the National Natural Science Foundation of China under Grant 61462031 and Grant 61662026, in part by the Natural Science Foundation of Jiangxi Province under Grant 20151BAB207033 and Grant 20161ACB21015, and in part by the Project of the Education Department of Jiangxi Province under Grant KJLD14031 and Grant GJJ150461. The associate editor coordinating the review of this manuscript and approving it for publication was Prof. Khan M. Iftekharuddin. (Corresponding author: Yong Yang.)

- S. Huang and J. Sun are with the School of Software and Communication Engineering, Jiangxi University of Finance and Economics, Nanchang 330032, China (e-mail: shuyinghuang2010@126.com; super_sun93@163.com).
- Y. Yang, Y. Fang, and Y. Que are with the School of Information Technology, Jiangxi University of Finance and Economics, Nanchang 330032, China (e-mail: greatyangy@126.com; leo.fangyuming@foxmail.com; qki120@163.com).
- P. Lin is with the College of Biomedical Engineering, South-Central University for Nationalities, Wuhan 430074, China (e-mail: tiger.lin9906@gmail.com).

Color versions of one or more of the figures in this paper are available online at http://ieeexplore.ieee.org.

Digital Object Identifier 10.1109/TIP.2018.2809472

size or increase the chip size of the sensors, which would generate shot noise degrading the image quality and increasing the cost, respectively [4]. To overcome these limitations, many studies try to use signal processing techniques to generate HR images by LR images. This process is called image super-resolution (SR) reconstruction [2]. Generally, image SR reconstruction aims to estimate a HR image from one or more observed low-resolution (LR) image frames based on reasonable assumptions or prior knowledge of the image generation model [5]. The SR problem was first studied by Tsai *et al.* in 1980s [6] and is regarded as an ill-posed problem [4]. During the past decades, various image SR methods have been proposed to deal with this conditionally insufficient problem [2], [3], [5]–[10].

Image SR reconstruction methods can be categorized as multi-frame image SR methods [11]-[14] and single-image SR methods [7]-[10], [15]-[17]. The multi-frame image SR method can be divided into two basic types of methods: frequency domain methods and spatial domain methods [13]. The frequency domain methods aim to eliminate spectrum aliasing and reconstruct the high frequency information, including Fourier Transform-based methods [6], Discrete Cosine Transform-based methods [18] and wavelet transform-based methods [19]. Though these methods are computationally efficient, the frequency domain methods are limited to model the image degradation process and have difficulty to use image prior knowledge [1]. To overcome these limitations, many spatial domain methods have been designed by making use of complicated global motion, local motion and optical blurring to establish a comprehensive observation model for image degradation processing. The spatial domain methods such as non-uniform interpolation method [20], iterative back projection (IBP) method [21] and projection onto convex sets (POCS) [22] are popular in image SR due to their good reconstruction ability. The drawback of the spatial domain methods are generally computationally expensive [11]. Furthermore, in practical applications, it is not easy to obtain an adequate number of LR images, and to estimate a HR image from multiple blurred and noisy images [23]. Therefore, compared with multi-frame image SR methods, single-image SR methods are much more desired in practical applications.

Single-image SR methods can be further divided into interpolation-based methods [24]–[26], reconstruction-based methods [27], [28] and example learning-based methods [16], [29]–[31]. Interpolation-based methods use the values of the adjacent pixels to estimate the values of interpolated

pixels. The interpolation-based methods are comparatively simple and have the advantage of relatively low computational complexity [2], [16]. However, the interpolation-based methods usually tend to generate the reconstructed HR images with edge halos and artifacts [4], [7].

Reconstruction-based methods [28], [32] generate a HR image based on designed degradation model. Based on maximum a posteriori (MAP) theory which forces some prior constraints into the cost function, the SR problem turns out to be well posed [1]. With the MAP theory by image prior constrains, the SR problem can be transformed into a minimization problem as $x = \arg\min[L(y, x) + \lambda U(x)],$ where $L(\cdot)$ is the data fidelity term that represents the degree of consistency between the HR image x and LR image y, $U(\cdot)$ is the regularization term describing the prior information of the original image, and λ is the regularization parameter, which is used to weight the contribution given by $L(\cdot)$ and $U(\cdot)$ during the processing [13]. This type of SR methods make use of image prior knowledge or reconstruction constraints to regularize the solution. Various kinds of priors have been incorporated into reconstruction-based methods, e.g., edge prior [33], gradient prior [34], non-local means priors [27], [35] and sparsity priors [16], [36]–[41]. The combination of different types of prior knowledge makes a better model for characterizing various image features and benefits the SR performance. However, reconstruction-based methods usually smear out image details, resulting in the loss of fine structures and overly smooth reconstruction results [3], [7].

In contrast to the above methods, the example learningbased methods estimate the HR image from the LR image by learning the relationship between the HR and LR image patches from the sample database [8]. These methods build a suitable training set and make full use of image priors to reduce edge halos and artifacts effectively. Therefore, we mainly focus on the study of the example learningbased SR method in this paper. Recently, a variety of example learning-based methods for SR image reconstruction have been proposed to obtain better SR results than conventional approaches. Timofte et al. [30] proposed the anchored neighborhood regression (ANR) scheme by sparse dictionary learning and used global collaborative coding for fast SR reconstruction. Yang et al. [36] used the sparse representation to reconstruct the HR image. This method learns two compact dictionaries by jointly training from the LR and HR image patch pairs, and assumed that the LR and LR image patches have the same sparse representation coefficients. Dong et al. [37] proposed an adaptive sparse domain select (ASDS) and adaptive regularization image SR scheme by sparse representation. A set of autoregressive models and nonlocal self-similarity are used as regularization terms in the sparse representation model to further improve the reconstruction quality. Peleg and Elad [38] proposed a single image SR method using a statistical prediction model based on sparse representation. Zeyde et al. [42] used K-SVD [43] for dictionary training and principal component analysis (PCA) to decrease the dimension of the LR image patches. Dong et al. [44] proposed a non-locally centralized sparse representation (NCSR) method by introducing the

sparse coding noise (SCN) and nonlocal self-similarity into the sparse model. Recently, Dong *et al.* [10] used a deep convolution neural network to learn mappings between LR and HR images and obtained excellent reconstruction quality. Although various types of SR reconstruction methods have been proposed to solve the ill-posed inverse problem in SR, they might produce undesired artifacts in HR images [41]. In particular, the SR performance becomes poor when the SR methods are conducted on blurred and noisy LR images.

It is known that the key of the SR problem is to recover the loss details of HR images and preserve image edges. In this paper, we propose a novel robust image edge-preserving smoothing super-resolution (REPS-SR) method based on the adaptive edge-preserving smoothing (EPS) regularization term. Specifically, the gradient domain guided image filtering [45] which has the property of edges preserving and smoothing is employed to design an EPS regularization in the proposed method. To the best of our knowledge, this is the first attempt to use gradient domain guided filter in image SR. Besides, K-means clustering and PCA are used to learn a compact dictionary. The proposed REPS-SR method uses the non-locally centralized sparsity and EPS regularization term as regularized terms to formulate a constrained optimization problem that can be solved by an iterative shrinkage algorithm [46]. The main contributions of this work over current methods can be summarized as follows.

- A novel robust image SR reconstruction method, i.e., REPS-SR, is presented for single image SR by EPS regularization.
- 2) The EPS regularization term is designed and incorporated into the sparse model to preserve image edges and reduce the noise in the reconstructed image.
- 3) A smoothing-aware factor is adaptively determined without manual interference by the estimation of unknown noise level to obtain an optimal balance between the data fidelity and the proposed EPS regularization term.

The remainder of this paper is organized as follows. In Section II, we review the related work of sparse representation theory. Section III introduces the model of the proposed REPS-SR method in detail. In Section IV, we present extensive experiments and corresponding analysis. The conclusion is summarized in Section V.

II. RELATED WORK

The image observation model describes the relationship between the original and observed images. In the image SR problem, the original and observed images are corresponding to HR and LR images, respectively. The image SR reconstruction aims to obtain the HR image from the degraded LR image. The problem of image SR reconstruction can be generally modeled as

$$y = \mathbf{H}x + v,\tag{1}$$

where **H** is a degradation matrix that represents blurring and a down-sampling operator, x is the original image, y is the observed image and v is the additive noise. Due to the insufficient condition of the SR problem, recovering HR image

might be not unique. To solve this ill-posed problem, many solutions have been proposed for single image SR problem in the past decades [8]–[10], [29]–[42]. Recently, there have been a large number of studies on sparse representation for the image SR problem.

The sparsity prior has been found to be a good image prior and has attracted great attention for image SR problem [17], [32], [39]–[44]. Researchers have found that nature image patches or signals could be sparsely represented as a sparse linear combination with respect to a dictionary, such as a DCT, wavelet or curvelet dictionary. The basic idea of sparse representation is as follows:

$$x \approx \Phi \alpha$$
, (2)

where $x \in \mathbb{R}^{m*1}$ is an original image patch or signal, $\Phi \in \mathbb{R}^{m*K}$ is an over-complete dictionary of K atoms, $\alpha \in \mathbb{R}^{K*1}$ is a vector where most coefficients in α have few nonzero entries. The sparse coefficients of x can be obtained by solving an l_0 -minimization optimization problem formulated as

$$\widehat{\alpha}_x = \arg\min \|\alpha\|_0, \quad \text{s.t. } x \approx \Phi\alpha,$$
 (3)

where $\|\alpha\|_0$ denotes the number of non-zeros in α . However, the l_0 -minimization is an NP-hard optimization problem [4]. It is suggested that as long as the desired coefficients α are sufficiently sparse, the problem can be efficiently solved by its approximate l_1 -minimization [36], as follows:

$$\widehat{\boldsymbol{\alpha}}_{x} = \arg\min \|\boldsymbol{\alpha}\|_{1}, \quad \text{s.t. } \boldsymbol{x} \approx \boldsymbol{\Phi} \boldsymbol{\alpha}.$$
 (4)

The l_1 -minimization optimization problem can be similarly formulated as

$$\widehat{\alpha}_x = \arg\min\left\{ \|x - \Phi\alpha\|_2^2 + \lambda \|\alpha\|_1 \right\},\tag{5}$$

where λ is a constant which balances the sparsity of the solution and the fidelity of the approximation to x. In image SR problems, what we obtain is the degraded image y, and what we aim to recover is the original x from y. The problem can be well formulated by solving the l_1 -minimization as

$$\widehat{\alpha}_{y} = \arg\min\left\{ \|y - \mathbf{H}\boldsymbol{\Phi}\boldsymbol{\alpha}\|_{2}^{2} + \lambda \|\boldsymbol{\alpha}\|_{1} \right\}.$$
 (6)

Once the sparse coding α is obtained, the HR image x can be estimated by $\hat{x} = \Phi \hat{\alpha}_y$.

In sparse representation theory, the learning of dictionary Φ is of great importance. Although analytically designed dictionaries such as DCT, wavelet, curvelet and contourlet share the advantages of being efficient and fast in image SR problems, they lack the adaptive ability for different image structures. Recently, various types of example-based dictionary learning methods have shown promising performance for image sparse representation [35]–[37]. These schemes aim to learn over-complete dictionaries which are redundant for representing various complex structures in natural images. However, sparse coding over a highly over-complete dictionary is unstable [44] and may cause visual artifacts [2]. Apart from the methods above, researchers have proposed adaptive dictionary learning methods which learn dictionaries from a set of example image patches. Yang *et al.* [47]

Algorithm 1 Pseudocode of the REPS-SR-Based Single Image Super-Resolution

Input: a LR image y and magnification factor.

Output: a HR image x.

- 1. Initialization:
- (a) Set the initial estimation \hat{x} by bicubic interpolation for image super-resolution;
- (b) Set the initial parameters λ_1 , δ and c. Estimate the unknown noise level according to [49] and adaptively determine the smoothing-aware factor λ_2 using Eq. (15).
- 2. Outer loop (dictionaries learning and clustering): iterate on t = 1 to T
- (a) Update the dictionaries $\{\Phi_k\}$ via *K*-means clustering and PCA;
- (b) Inner loop: for each iteration j = 1 to J do
 - 1) Compute the gradient domain guided image filtering image $\hat{x}_{G}^{(t)}$ by Eq. (10);
 - 2) Update $\hat{x}^{(t+1/2)}$ by Eq. (11), where δ is a pre-determined constant;
 - 3) Compute the sparse coding coefficients of each patch by Eq. (13), where Φ_k is the dictionary assigned to patch $\hat{x}_i = \mathbf{R}_i \hat{x}^{(t+1/2)}$;
 - 4) Update the sparse coding $\alpha_i^{(t+1)}$ by using the iterative shrinkage operator given in Eq. (14);
 - 5) Update the regularization parameter λ_1 and the nonlocal means $\boldsymbol{\beta}_i$ according to [44], if $mod(j, j_0) = 0$.
 - 6) Reconstruct the estimated image by using Eq. (8);
- (c) Update the HR image by $\hat{x} = \hat{x}^{(t+1)}$.

clustered HR image patches into several groups of geometric patches to learn its correspondingly geometric clustered dictionaries and the clustering aggregation scheme is used to estimate original image patches. In this paper, a more compact clustering PCA dictionary is learned according to the NCSR [44] method. In the next section, the proposed REPS-SR algorithm is presented which includes dictionary learning scheme, the model of the proposed method and the optimizing algorithm.

III. PROPOSED REPS-SR ALGORITHM

In this section, we introduce the proposed REPS-SR algorithm in detail. Firstly, the *K*-means clustering and PCA are used to learn sub-dictionaries from LR images. Then, the proposed EPS regularization term is introduced to preserve the edges of the reconstructed image and remove artifacts. An adaptive smoothing-aware factor determination scheme is proposed and the iterative shrinkage algorithm is used to solve the SR problem. The procedure of the proposed REPS-SR method is summarized in **Algorithm 1**.

TABLE I

AVERAGE PSNR (dB)/SSIM RESULTS ON SIX TEST IMAGES WITH DIFFERENT PARAMETERS

λ_2		Noise level σ											
702	0	1	2	3	4	5	6	7	8	9	10		
0	29.8900 0.8735	28.9167 0.8472	29.1450 0.8467	29.0333 0.8376	28.8083 0.8273	28.5400 0.8165	28.2800 0.8060	28.0333 0.7947	27.7583 0.7838	27.5200 0.7730	27.2767 0.7617		
0.1	29.9583 0.8715	28.9550 0.8525	29.2033 0.8529	29.0967 0.8441	28.8550 0.8334	28.5950 0.8222	28.3233 0.8112	28.0650 0.8001	27.7950 0.7882	27.5500 0.77685	27.3017 0.7648		
0.2	29.8850 0.8585	28.9883 0.8520	29.2350 0.8533	29.1267 0.8455	28.8850 0.8354	28.6150 0.8248	28.3483 0.8145	28.1000 0.8039	27.8003 0.7925	27.5783 0.7812	27.3333 0.7693		
0.3	29.7533 0.8457	28.9900 0.8501	29.2400 0.8526	29.1333 0.8456	28.8950 0.83591	28.6367 0.8260	28.3700 0.8160	28.1150 0.8060	27.8517 0.7954	27.6050 0.7847	27.3617 0.7738		
0.4	29.5600 0.8297	28.9750 0.8479	29.2417 0.8514	29.1383 0.8449	28.9000 0.83593	28.6366 0.8262	28.3766 0.8168	28.1367 0.8072	27.8667 0.7968	27.6667 0.7869	27.3867 0.7766		
0.5	29.3800 0.8167	28.9450 0.8450	29.2333 0.8500	29.1383 0.8444	28.9017 0.8355	28.6383 0.8259	28.3850 0.8169	28.1317 0.8075	27.8800 0.7978	27.6400 0.7882	27.4000 0.7787		
0.6	29.1950 0.8053	28.9067 0.8421	29.2183 0.8483	29.1250 0.8432	28.8950 0.8349	28.6386 0.8254	28.3833 0.8167	28.1366 0.80768	27.8833 0.8015	27.6500 0.7891	27.4100 0.7799		
0.7	29.0333 0.7959	28.8667 0.8393	29.18667 0.8461	29.1117 0.8419	28.8817 0.8340	28.6267 0.8248	28.3883 0.8173	28.1383 0.80768	27.8783 0.7982	27.6567 0.7898	27.4233 0.7809		
0.8	28.8867 0.7869	28.8150 0.8353	29.1650 0.8439	29.0933 0.8404	28.8767 0.8332	28.6233 0.8243	28.3817 0.8160	28.1393 0.8077	27.8783 0.7984	27.6550 0.7899	27.4333 0.7814		
0.9	28.6783 0.7785	28.7583 0.8308	29.1333 0.8411	29.0733 0.8384	28.8617 0.8316	28.6183 0.8235	28.3767 0.8154	28.1333 0.8070	27.8850 0.7989	27.6583 0.78995	27.4333 0.7817		
1	28.5117 0.7694	28.7050 0.8261	29.1050 0.8387	29.0617 0.8364	28.8483 0.8301	28.6133 0.8222	28.3683 0.8144	28.1350 0.8065	27.8887 0.7980	27.6583 0.78998	27.4355 0.78175		
1.1	28.4017 0.7649	28.6517 0.8210	29.0817 0.8368	29.0400 0.8346	28.8267 0.8285	28.5950 0.8204	28.3633 0.8135	28.1200 0.8047	27.8750 0.7964	27.6566 0.78996	27.4367 0.78176		
1.2	28.2817 0.7581	28.6100 0.8196	29.0500 0.8350	29.0233 0.8334	28.8200 0.8274	28.5850 0.8191	28.3450 0.8117	28.1183 0.8034	27.8650 0.7951	27.6517 0.7878	27.4350 0.7818		

A. Learning the Self-Example Sub-Dictionaries

Learning a representative dictionary is a critical issue in sparse representation modeling. In the proposed REPS-SR model, a series of sub-dictionaries are learned to code various image structures. In contrast to the ASDS method [37], we learn the sub-dictionaries from the image itself which makes the proposed REPS-SR method more adaptive for different images. In the proposed method, we first extract image patches from image x. In order to learn a series of sub-dictionaries to code various local image structures, a set of image patches will be selected to be involved in the dictionary learning process. The image patch is selected when its intensity variance is greater than a threshold Δ . This patch selection criterion tries to exclude the smooth patches from training and guarantees that only these patches including a certain amount of edge structures are used to learn the dictionary. Suppose that M image patches $X = [x_1, x_2, ... x_M]$ are selected, we have to learn K sub-dictionaries from X so that the most relevant sub-dictionaries can be selected adaptively for the local image patches. The image patches are clustered into K clusters and we learn a compact dictionary from each cluster. To make the dictionaries representative for image edges and local structures, the high-pass filtering is used to

process the entire set of image patches before clustering. The K-means algorithm is adopted to cluster the high-pass filtered image patches into K clusters. Since learning an over-complete dictionary is computationally costly, a compact dictionary is learned using PCA for the reason that the patches in a cluster tend to have similar structures and redundancy information. \mathbf{S}_k denotes the sub-dataset after high-pass filtering and K-means algorithm, and Ω_k denotes the co-variance matrix of \mathbf{S}_k . By applying PCA to Ω_k , an orthogonal transformation matrix \mathbf{P}_k can be obtained. Then, let \mathbf{P}_k be the dictionary of \mathbf{S}_k and $\alpha_k = \mathbf{P}_k^T \mathbf{S}_k$ be the sparse representation coefficient, an approximate solution of the objective function can be obtained:

$$(\mathbf{\Phi}_k, \boldsymbol{\alpha}_k) = \arg\min\left\{ \|\mathbf{S}_k - \mathbf{\Phi}_k \, \boldsymbol{\alpha}_k\|_F^2 + \lambda \, \|\boldsymbol{\alpha}_k\|_1 \right\}. \tag{7}$$

With the scheme described above, the K sub-dictionaries of \mathbf{S}_k are finally learned. $\mathbf{\Phi}_k$ is constructed by $\mathbf{\Phi}_k = [\mathbf{P}_1, \mathbf{P}_2, \dots \mathbf{P}_k]$. Once the over-complete dictionary $\mathbf{\Phi}_k$ and sparse code α_k are obtained, each image patch can be well represented by Eq. (2). In the proposed REPS-SR scheme, we adaptively select one sub-dictionary from the K-means PCA dictionaries to code it, leading to a stable and sparse representation of the given patch. The image \mathbf{X} can be reconstructed by making use of all the image patch information. The approximate

and straightforward least-square solution can be formulated as follows:

$$\widehat{\mathbf{X}} = \left(\sum_{i=1}^{N} \mathbf{R}_{i}^{T} \mathbf{R}_{i}\right)^{-1} \sum_{i=1}^{N} \left(\mathbf{R}_{i}^{T} \mathbf{\Phi} \boldsymbol{\alpha}_{x,i}\right), \tag{8}$$

where \mathbf{R}_i is the matrix that extracting patch \mathbf{x}_i from the image \mathbf{x} ; N is the number of image patches; and $\alpha_{x,i}$ is the sparse coefficient of each image patch over the sub-dictionary Φ_k . After learning dictionary Φ_k , we propose to design the REPS-SR model. The detailed algorithm of the proposed SR model is presented in the next subsection.

B. Proposed REPS-SR Model

Here, we propose to use the REPS-SR method to solve the single-image SR problem. Since image patches often contain repetitive patterns, such nonlocal redundancy is very helpful for improving the reconstruction performance of images. The nonlocal self-similarity is used as a regularization term to provide a good estimation of α_i . Meanwhile, considering that image edges convey abundant image information, we use the image edges as a regularization term to constrain the image SR model. Here, an EPS regularization is designed to be incorporated into the sparse model. In the REPS-SR model, the reconstructed image \hat{x} at each iteration is regarded as the guidance image and the input filtering image. During iterative processing, the proposed EPS regularization term constrains the reconstructed HR image close to the filtered image which is an edge-preserving smoothing image. The reconstructed image edges can be preserved and the noise can be reduced. Furthermore, the edges of reconstructed images can be enhanced after multiple iterations. Mathematically, the proposed REPS-SR model for the single image SR problem can be formulated as follows:

$$\widehat{\boldsymbol{\alpha}}_{y} = \arg \min \left\{ \begin{aligned} & \left\| y - \mathbf{H} \boldsymbol{\Phi} \boldsymbol{\alpha} \right\|_{2}^{2} \\ & + \lambda_{1} \sum_{i} \left\| \boldsymbol{\alpha}_{i} - \boldsymbol{\beta}_{i} \right\|_{1} \\ & + \lambda_{2} \left\| \widehat{\boldsymbol{x}} - \boldsymbol{x}_{G} \right\|_{2}^{2} \end{aligned} \right\}. \tag{9}$$

On the right side of Eq. (9), the first term is data fidelity of the solution; the second is a non-local self-similar regularization term; the third is the proposed EPS regularization term. α_i is the sparse coefficient of each image patch x_i over the dictionary Φ ; β_i is the nonlocal means of α_i [44] in the sparse coding domain; λ_1 and λ_2 are the regularization parameters; x_G is the output image by the gradient domain guided filtering, which can be calculated as follows:

$$\widehat{\mathbf{x}}_{G}^{(t)} = \bar{a}_{p} \,\widehat{\mathbf{x}}^{(t)} + \bar{b}_{p},\tag{10}$$

where $\bar{a}_p = \frac{1}{|\Omega_{\zeta 1}|} \sum_{p' \in \Omega_{\zeta 1}(p)} a_{p'}$ and $\bar{b}_p = \frac{1}{|\Omega_{\zeta 1}|} \sum_{p' \in \Omega_{\zeta 1}(p)} b_{p'}$ are the average of $a_{p'}$ and $b_{p'}$ [45]. Here, $\widehat{x}^{(t)}$ is the guidance image and $\widehat{x}_G^{(t)}$ is the filtering output image. In the next subsection, we propose to use iterative shrinkage algorithm [46] to optimize the proposed REPS-SR model.

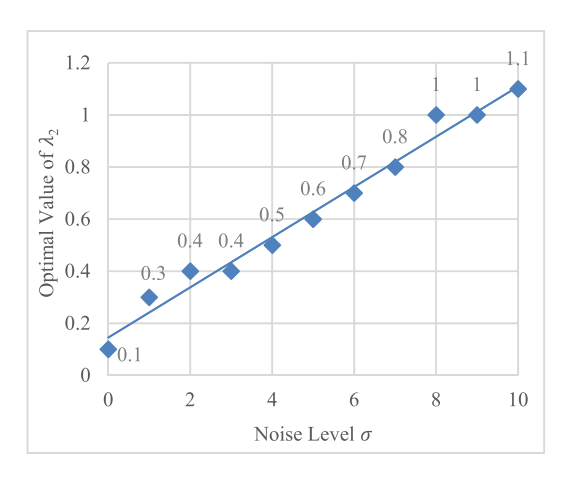


Fig. 1. The optimal value of λ_2 for different noise levels.

C. Iterative Shrinkage Algorithm

As the SR problem is non-convex, it is difficult to pursue an exact solution. In the proposed method, an iterative shrinkage algorithm is used to solve REPS-SR objective function in Eq. (9). We first update the HR image x using the gradient descent method as follows:

$$\widehat{\mathbf{x}}^{(t+1/2)} = \widehat{\mathbf{x}}^{(t)} + \delta \left(\frac{\mathbf{H}^T \left(\mathbf{y} - \mathbf{H} \widehat{\mathbf{x}}^{(t)} \right)}{+ \lambda_2 \left(\widehat{\mathbf{x}}^{(t)} - \widehat{\mathbf{x}}_G^{(t)} \right) \left(\widehat{\mathbf{x}}^{(t)} - \widehat{\mathbf{x}}_G^{(t)} \right)'} \right), \quad (11)$$

where δ is a small constant and $\widehat{x}^{(t)}$ is the current estimation of the HR image. $\widehat{x}_G^{(t)}$ is the output image by gradient guided filtering. By substituting Eq. (10) into Eq. (11), we obtain

$$\widehat{\mathbf{x}}^{(t+1/2)} = \widehat{\mathbf{x}}^{(t)} + \delta \left(\mathbf{H}^T \left(\mathbf{y} - \mathbf{H} \widehat{\mathbf{x}}^{(t)} \right) + \lambda_2 \left(a_p^T - 1 \right) \left(\widehat{\mathbf{x}}^{(t)} - \widehat{\mathbf{x}}_G^{(t)} \right) \right). \tag{12}$$

Then the sparse coding coefficients α_i can be updated as follows:

$$\boldsymbol{\alpha}_{i}^{(t+1/2)} = \boldsymbol{\Phi}_{k}^{T} \, \mathbf{R}_{i} \, \hat{\boldsymbol{x}}^{(t+1/2)}, \tag{13}$$

where Φ_k denotes the PCA dictionary of a cluster obtained by K-means clustering. With the updated α_i , the non-local self-similar sparse coefficients β_i can be estimated according to reference [44]. To further estimate the sparse coding coefficient α_i , an iterative shrinkage operator is selected and the updating processing can be formulated in the following form:

$$\boldsymbol{\alpha}_{i}^{(t+1)} = S_{\tau} \left(\frac{\boldsymbol{\Phi}^{T} \mathbf{H}^{T} \left(\mathbf{y} - \mathbf{H} \boldsymbol{\Phi} \, \boldsymbol{\alpha}_{i}^{(t+1/2)} \right) / c}{+ \boldsymbol{\alpha}_{i}^{t+1/2} - \boldsymbol{\beta}_{i}} \right) + \boldsymbol{\beta}_{i}, \quad (14)$$

where S_{τ} is the classic soft-thresholding operator, and c is an auxiliary parameter guaranteeing the convexity of the shrinkage function. With the updating sparse coding coefficient α_i , HR image patches are updated by $x_i^{(t+1)} = \Phi_k \alpha_i^{(t+1)}$. Finally, the whole HR image can be reconstructed by averaging all of the reconstructed patches in Eq. (8).



Fig. 2. Twelve images in our experiments.

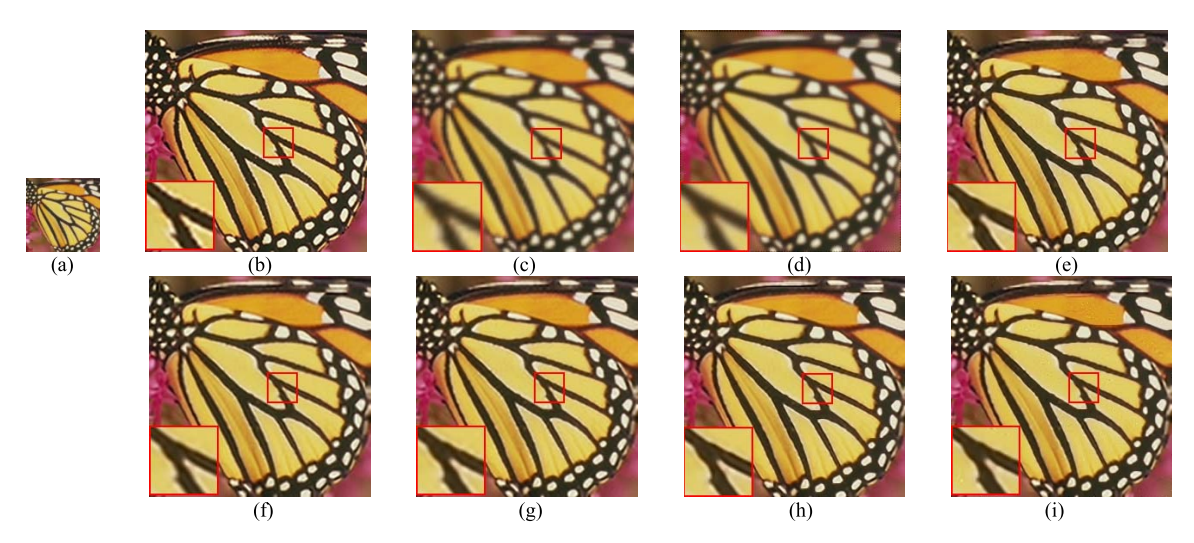


Fig. 3. Visual comparison samples of the proposed method and other state-of-the-art methods on 'Butterfly' image with a scale factor of 3, noise level $\sigma = 0$. (a) LR. (b) original. (c) Bicubic. (d) NARM. (e) MSEPLL. (f) ASDS. (g) NCSR. (h) SMSR. (i) REPS-SR.

TABLE II PSNR (dB)/SSIM Results on the Reconstruction of HR Images With a Scale Factor of 3, Noise Level $\sigma=0$

Images	REPS-SR	SMSR[3]	NCSR[44]	ASDS[37]	MSEPLL[40]	NARM[41]	Bicubic
Butterfly	28.51 /0.9024	28.34/ 0.9243	28.08/0.9159	27.35/0.9057	28.14/0.9142	22.61/0.7856	20.78/0.7175
Flower	29.59/0.8530	29.65/0.8610	29.50/0.8564	29.18/0.8466	29.02/0.8392	25.52/0.7124	24.83/0.6753
Hat	31.39/0.8631	31.60/0.8771	31.27/0.8703	31.01/0.8717	30.94/0.8583	27.31/0.7931	27.20/0.7778
Parrots	30.51/0.9077	30.81/0.9188	30.47/0.9147	30.10/0.9099	30.04/0.9076	26.15/0.8399	25.58/0.8261
Plants	34.10/0.9169	34.22/0.9208	34.04/0.9189	33.42/0.9074	33.15/0.8983	28.95/0.8120	27.83/0.7875
Leaves	28.14 /0.9174	27.80/ 0.9306	27.44/0.9216	26.94/0.9096	26.35/0.8984	21.51/0.7469	19.83/0.6411
Ppt	25.75 /0.8942	24.17/0.9059	25.16/0.9048	24.71/0.8987	25.17/ 0.9069	21.09/0.7883	19.98/0.7455
Parthenon	27.23/0.7454	27.24/0.7551	27.18/0.7507	26.89/0.7367	26.95/0.7397	24.70/0.6359	24.12/0.6205
Bird	35.86 /0.9530	35.77/ 0.9596	35.80/0.9570	35.53/0.9536	35.21/0.9487	29.24/0.8645	27.53/0.8363
Eyetest	23.20 /0.8779	20.73/0.8884	21.69/0.8892	20.20/0.8508	22.36/ 0.9078	17.76/0.7696	16.59/0.7129
Comic	25.35/0.7888	25.38/0.8014	25.31/0.7974	25.16/0.7895	25.19/0.7856	22.20/0.6174	21.40/0.5782
Starfish	29.32/0.8674	29.51/0.8783	29.25/0.8727	28.88/0.8676	28.73/0.8588	24.78/0.7291	23.86/0.6942
Average	29.08 /0.8739	28.77/ 0.8851	28.77/0.8808	28.28/0.8707	28.44/0.8720	24.32/0.7579	23.29/0.7177

D. Adaptive Smoothing-Aware Factor

In the proposed REPS-SR model, the regularization parameter λ_1 controls the tradeoff between the fidelity to data and the nonlocal regularization, and λ_2 controls the smoothness of the solution. A suitable choice of regularization parameter is beneficial to obtain a global optimal solution and improve the convergence rate. Dong *et al.* [44] proposed to use the MAP

estimator to adaptively determine the regularization parameter λ_1 which gets good SR performance. In the proposed method, the determination of λ_1 uses the same scheme as the NCSR model. To make our method more competitive, we propose to adaptively obtain the smoothing-aware factor λ_2 . In the SR problem, a large value of the regularization parameter will be used when the number of LR images is small or the fidelity of the observed data is low, which might be caused

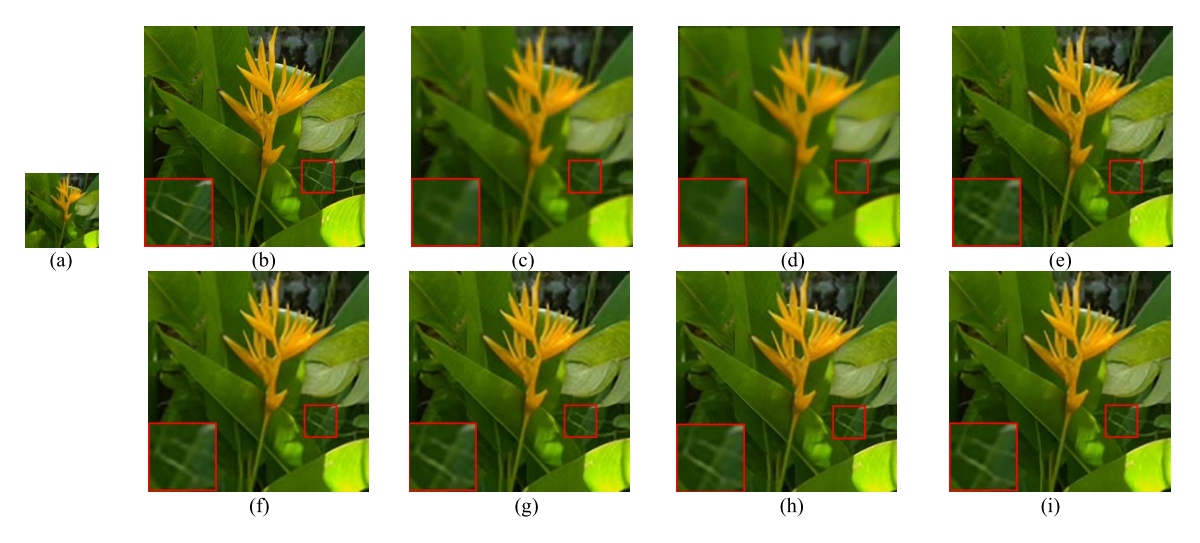


Fig. 4. Visual comparison samples of the proposed method and other state-of-the-art methods on '*Plants*' image with a scale factor of 3, noise level $\sigma = 0$. (a) LR. (b) original. (c) Bicubic. (d) NARM. (e) MSEPLL. (f) ASDS. (g) NCSR. (h) SMSR. (i) REPS-SR.

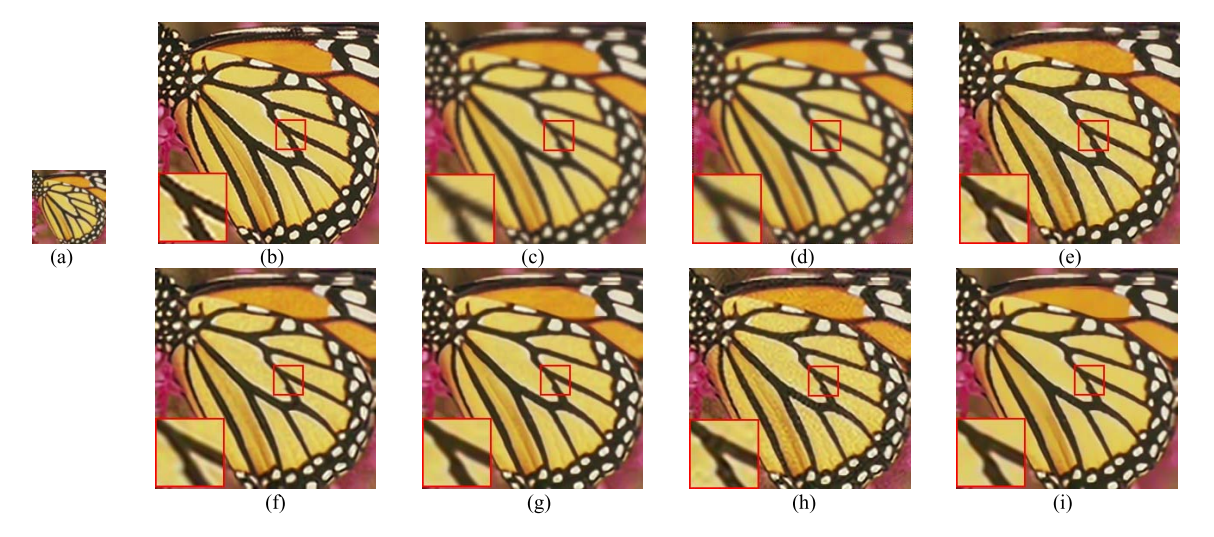


Fig. 5. Visual comparison samples of the proposed method and other state-of-the-art methods on 'Butterfly' image with a scale factor of 3, noise level $\sigma = 5$. (a) LR. (b) original. (c) Bicubic. (d) NARM. (e) MSEPLL. (f) ASDS. (g) NCSR. (h) SMSR. (i) REPS-SR.

by registration error or noise [4]. On the other hand, a small parameter will lead to a good solution of the SR problem when the noise level is small. It means that a higher level of noise level should be corresponding to a larger value of regularization parameter [36]. In the proposed method, we adaptively determine the smoothing-aware factor λ_2 by regarding the factor λ_2 as a function of unknown noise level. In this paper, the noise level of LR image is estimated based on the selected weak textured patches [49], [50] using PCA. Many experiments were conducted to verify the generality of the theory that a high level of noise corresponds to a large value of λ_2 . Different levels of Gaussian noise are added to various images, and different values of λ_2 that range from 0 to 2 are used in our experiments to obtain a large number of SR results. Table I shows the average experimental results when noise level ranges from 0 to 10 and λ_2 ranges from 0 to 1.2 with six test images. As seen from Table I, for a fixed noise level, a more suitable value of λ_2 can be found according to the SR results considering both the peak signal

to noise ratio (PSNR) and structural similarity (SSIM) [51] values. Fig. 1 shows the relationship between optimal values of λ_2 and their corresponding noise levels, which verifies that the smoothing-aware factor λ_2 increases as the noise level increases. From Fig. 1, we propose to define a function to fit the statistical relationship between unknown noise level and the smoothing-aware factor λ_2 , which is formulated as follows:

$$\lambda_2 = m\sigma + n = m \sqrt{\lambda_{\min}\left(\frac{1}{N}\sum_{i=1}^{N} (\mathbf{y'}_i - \mu) (\mathbf{y'}_i - \mu)^T\right) + n},$$
(15)

where $\sigma = \sqrt{\lambda_{\min}(\sum_{\mathbf{y}'})}$ is the estimated noise level, $\sum_{\mathbf{y}'} = \frac{1}{N} \sum_{i=1}^{N} \left(\mathbf{y}'_i - \mu\right) \left(\mathbf{y}'_i - \mu\right)^T$ denotes the covariance of selected weak textured patches \mathbf{y}'_i , N is the number of patches \mathbf{y}'_i and μ is the average of image patches, and m and n are the fitted variables, with corresponding values of 0.1 and 0.1,

respectively. Applying the above scheme, for nature image SR, once the noise level is estimated, we can adaptively determine the smoothing-aware factor λ_2 , the experimental results show better SR performance of the proposed method than that with a fixed constant.

IV. EXPERIMENT RESULTS

To validate the effectiveness of the proposed REPS-SR method, numerous experiments are conducted on a variety of natural images in this section. The images used in the proposed method are shown in Fig. 2. The basic parameter settings of the proposed REPS-SR method are as follows: the cluster number K is 70, the patch size is 6×6 with overlapping 4, $\delta = 7$, c = 0.35, T = 5, J = 160. In our experiments, the HR image is first blurred by using a 7×7 Gaussian kernel with a standard deviation of 1.6, and then the blurred image is down-sampled in both horizontal and vertical directions by a scaling factor of 3 to generate the LR image. In our experiments, H is assumed as a Gaussian matrix. Different levels of Gaussian noise are added to the LR image to verify the performance of the proposed method. We compare the proposed method with several state-of-theart methods, including Bicubic, MSEPLL [40], NARM [41], ASDS [37], NCSR [44], and SMSR [3]. Since human vision is more sensitive to the luminance component, all our experiments are carried out using only the luminance component, while the bicubic interpolator is applied to the chromatic components. The PSNR and SSIM [51] values are calculated in the luminance channel to evaluate the quality of our final SR images for the objective comparison of our REPS-SR method and the state-of-the-art methods.

A. Effectiveness and Robustness of the Proposed Method

In this subsection, we present the results from experiments on twelve images shown in Fig. 2 to evaluate the SR performance of the proposed method. Different levels of Gaussian noise are added to explore the robustness of the proposed method against noise. Tables II and III show the objective evaluation results of PSNR/SSIM when the added Gaussian noise levels are 0 and 5 and the magnification factor is 3. As seen from the results, the proposed REPS-SR method achieves slightly higher PSNR values and the SSIM value is very close to that of NCSR method when the noise level is 0. Since SMSR method [3] designs a multistep magnification scheme for the initial estimation of the HR image instead of bicubic interpolation, the performance of the proposed REPS-SR method is not as good as that of SMSR method. Figs. 3 and 4 show visual comparison examples of test images. It can be seen that the proposed REPS-SR method recover image edges better and show comfortable visual effects compared with SMSR method. However, when the noise level increases, our REPS-SR method achieves better results both in objective assessment and visual comparison. As seen from Table III, when the noise level is 5, the proposed REPS-SR method outperforms the existing competitive methods in objective evaluations for all test images. The subjective evaluation is shown in Figs. 5 and 6 with 'Butterfly' and

'Plants' as the example images. Since our method proposes to use the gradient guided filtering to form an edge-preserving regularization term, sharper edges and much smooth regions can be recovered. Compared with NCSR method [44] and SMSR method [3], our method can better preserve edges and the reconstructed image is much cleaner. It is noted that when the noise level gradually increases, worse SR results are obtained with all methods. Table IV shows the objective evaluation results of PSNR/SSIM values when the added Gaussian noise level is 10 with a magnification factor of 3 and the subjective visual effect is shown in Figs. 7 and 8. From those figures, we can see that when the noise is larger, the proposed method can better recover the HR image and suppress noise. Fig. 9 shows results of the proposed method and other state-of-the-art SR methods on 'Butterfly' image when the noise level gradually increases. The average performance on twelve test images is shown in Fig. 10. From those figures, we can see that the proposed method degrades more slowly compared with other SR methods. Among the existing methods, SMSR [3] and ASDS [37] degrade faster than other methods when the noise level increases. Our method achieves the highest PSNR/SSIM values when adding highlevel noise on test images. Our method also performs well with different noise levels, which indicates that the proposed REPS-SR method is robust to noise.

B. Discussion on the Proposed EPS Regularization

In the proposed method, the gradient guided filtering is used to preserve image edges and reduce noise in the smooth area. The gradient guided filtering is used to obtain the edgepreserving smoothing image. The filtering output image is calculated and incorporated into image SR model. The proposed EPS regularization makes the reconstructed HR images closer to the filtering output image which is helpful to minimize the objective function in Eq. (9). Furthermore, due to the gradient guided filtering, the images edges can be enhanced during iterative processing. The proposed EPS regularization term can also remove some noise in the reconstructed image. Moreover, the REPS-SR method makes the gradient of the reconstructed image similar to the gradient guided filtering output image. Experiments indicate that the proposed REPS-SR method achieve promising performance, especially for noisy images.

C. Investigation on the Smoothing-Aware Factor

In this subsection, we discuss the scheme that adaptively determines the smoothing-aware factor λ_2 . In the regularization-based SR methods, a fitted value of the regularization parameter is an essential issue. Instead of determining the parameter experiential, we propose to adaptively adjust the smoothing-aware factor λ_2 according to the noise level of LR images. Table V shows our experimental results with added noise levels 0, 5 and 10. For a fixed noise level, we conduct the experiments with $\lambda_2 = 0.3$, $\lambda_2 = 0.8$ and the adaptive method. From Table V, we can observe that when the added noise level is fixed, different values of λ_2 influence the SR results. Fig. 11 shows how λ_2 influences the visual

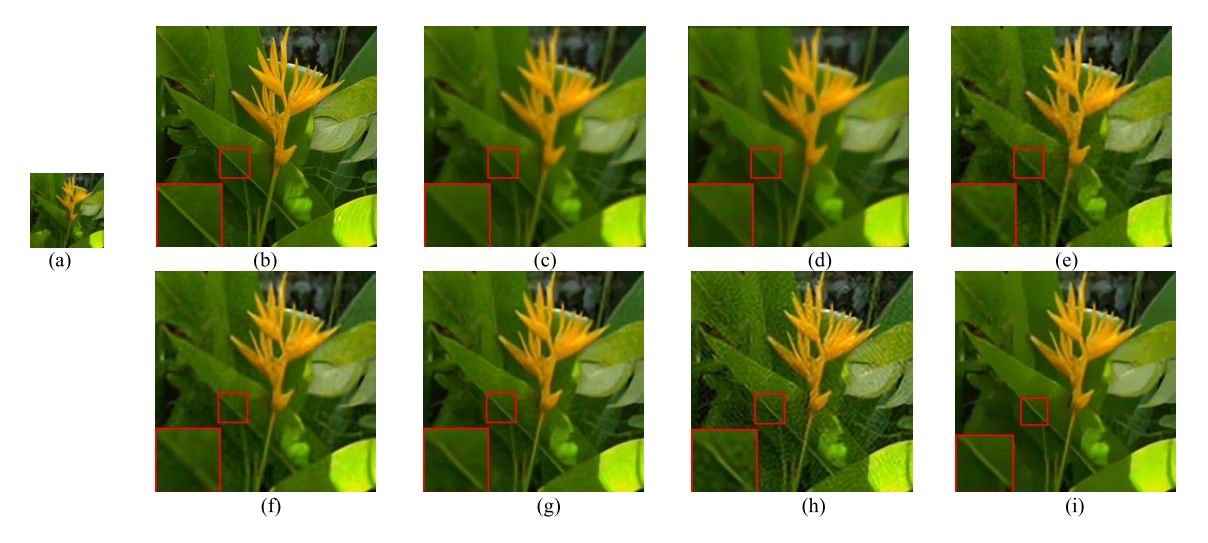


Fig. 6. Visual comparison samples of the proposed method and other state-of-the-art methods on '*Plants*' image with a scale factor of 3, noise level $\sigma = 5$. (a) LR. (b) original. (c) Bicubic. (d) NARM. (e) MSEPLL. (f) ASDS. (g) NCSR. (h) SMSR. (i) REPS-SR.

TABLE III PSNR (dB)/SSIM Results on the Reconstruction of HR Images With a Scale Factor of 3, Noise Level $\sigma=5$

Images	REPS-SR	SMSR[3]	NCSR[44]	ASDS[37]	MSEPLL[40]	NARM[41]	Bicubic
Butterfly	27.17/0.8932	26.44/0.8316	26.87/0.8869	26.00/0.8614	26.88/0.8737	22.60/0.7789	20.74/0.7039
Flower	28.26/0.8063	27.55/0.7397	28.12/0.7950	27.70/0.7745	27.83/0.7763	25.51/0.7038	24.74/0.6484
Hat	30.19/0.8352	29.07/0.7178	30.02/0.8229	29.57/0.8130	29.70/0.7941	27.41/0.7817	27.00/0.7482
Parrots	29.57/0.8836	28.69/0.7652	29.50/0.8742	28.75/0.8656	28.82/0.8487	26.06/0.8284	25.43/0.7982
Plants	31.99/0.8652	30.26/0.7643	31.79/0.8579	31.07/0.8349	30.18/0.8290	28.79/0.8001	27.62/0.7613
Leaves	26.67/0.9066	26.12/0.8662	26.29/0.8943	25.47/0.8631	25.31/0.8615	21.57/0.7430	19.80/0.6330
Ppt	25.12/0.9049	24.20/0.8242	24.85/0.8847	24.15/0.8685	24.64/0.8701	21.27/0.7915	19.95/0.7286
Parthenon	26.49/0.7090	26.08/0.6528	26.40/0.7003	26.07/0.6804	26.26/0.6830	24.70/0.6293	24.04/0.6045
Bird	33.01/0.9108	31.07/0.8269	32.88/0.9078	32.72/0.9017	32.50/0.8907	29.16/0.8572	27.31/0.8026
Eyetest	22.11/0.9140	21.62/0.8680	21.74/0.8949	20.49/0.8508	22.03/0.8914	18.04/0.7778	16.57/0.7038
Comic	24.59/0.7465	24.28/0.7168	24.51/0.7407	24.24/0.7233	24.39/0.7256	22.16/0.6100	21.35/0.5687
Starfish	27.86/0.8171	27.44/0.7787	27.79/0.8159	27.30/0.8042	27.48/0.8002	24.72/0.7199	23.75/0.6789
Average	27.75/0.8494	26.90/0.7794	27.56/0.8396	26.96/0.8201	27.17/0.8204	24.33/0.7518	23.19/0.6983

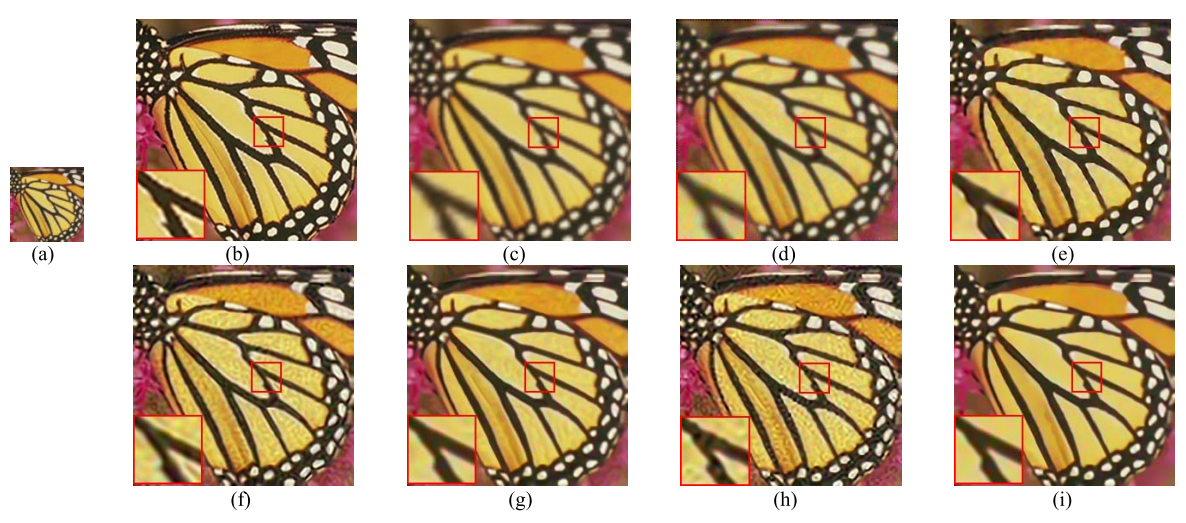


Fig. 7. Visual comparison samples of the proposed method and other state-of-the-art methods on 'Butterfly' image with a scale factor of 3, noise level $\sigma=10$. (a) LR. (b) original. (c) Bicubic. (d) NARM. (e) MSEPLL. (f) ASDS. (g) NCSR. (h) SMSR. (i) REPS-SR.

assessment with 'Butterfty' as the example image. It shows that using an optimal λ_2 with our method can achieve promising visual effects. Furthermore, we found that a fixed value of λ_2 may not be suitable for different noise levels. For example,

 $\lambda_2 = 0.6$ is relatively suitable when the noise level is 5. However, when the noise level is 10, the experimental results become worse. It can be seen from Table V that the proposed adaptive smoothing-aware scheme outperforms almost all the

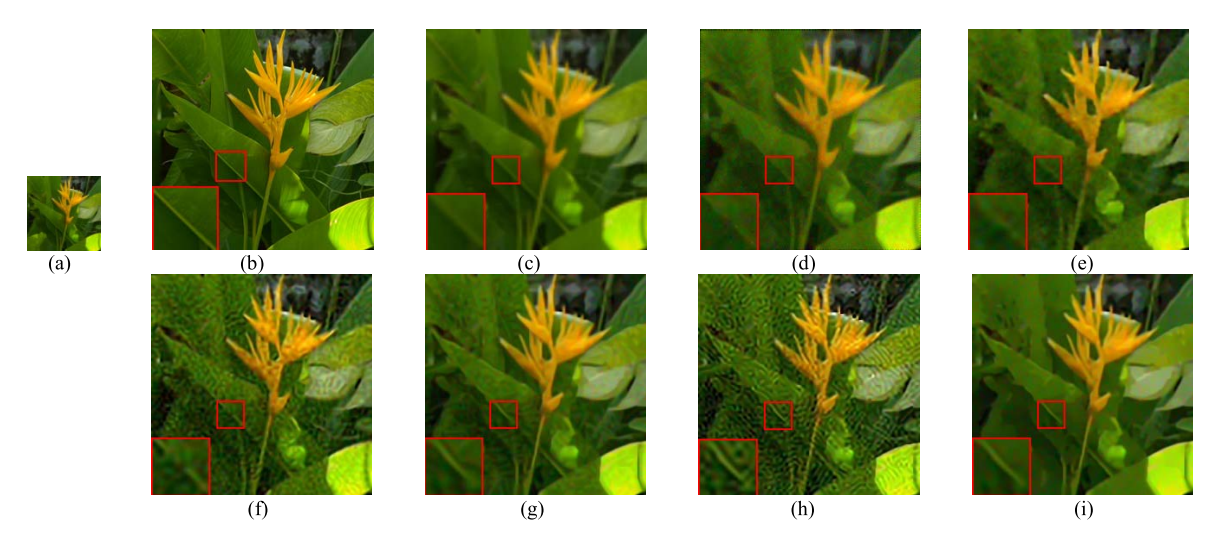


Fig. 8. Visual comparison samples of the proposed method and other state-of-the-art methods on 'Plants' image with a scale factor of 3, noise level $\sigma = 10$. (a) LR. (b) original. (c) Bicubic. (d) NARM. (e) MSEPLL. (f) ASDS. (g) NCSR. (h) SMSR. (i) REPS-SR.

TABLE IV PSNR (dB)/SSIM Results on the Reconstruction of HR Images With a Scale Factor of 3, Noise Level $\sigma=10$

Images	REPS-SR	SMSR[3]	NCSR[44]	ASDS[37]	MSEPLL[40]	NARM[41]	Bicubic
Butterfly	25.97/0.8657	24.30/0.7156	25.74/0.8495	24.62/0.7592	25.49/0.8469	22.42/0.7581	20.62/0.6693
Flower	27.10/0.7654	25.21/0.5955	26.94/0.7343	26.19/0.6694	26.59/0.7428	25.18/0.6767	24.45/0.6150
Hat	29.14/0.8066	26.26/0.5359	28.78/0.7649	27.57/0.6523	28.76/0.7764	27.03/0.7504	26.48/0.6778
Parrots	28.35/0.8567	25.95/0.5847	28.05/0.8209	27.08/0.7226	27.56/0.8258	25.78/0.7994	25.06/0.7300
Plants	30.49/0.8222	26.76/0.5815	30.20/0.8006	28.55/0.6963	29.62/0.7881	28.28/0.7670	27.04/0.6976
Leaves	25.28/0.8720	24.14/0.7833	25.07/0.8587	24.22/0.7916	23.98/0.8216	21.37/0.7269	19.70/0.6137
Ppt	24.51/0.8686	23.60/0.7138	24.30/0.8427	23.47/0.7934	23.91/0.8491	21.21/0.7732	19.85/0.6885
Parthenon	25.79/0.6745	24.34/0.5254	25.71/0.6528	24.09/0.5907	25.51/0.6444	24.51/0.6092	23.77/0.5639
Bird	30.90/0.8683	27.22/0.6685	30.69/0.8556	29.42/0.7822	30.51/0.8553	28.62/0.8303	26.76/0.7581
Eyetest	21.35/0.8843	21.04/0.7901	21.17/0.8690	20.10/0.7970	21.53/0.8864	17.95/0.7700	16.52/0.6794
Comic	23.61/0.6864	22.82/0.6143	23.56/0.6799	23.60/0.6546	23.35/0.6589	21.96/0.5869	21.20/0.5441
Starfish	26.45/0.7623	25.05/0.6176	26.40/0.7566	25.81/0.7165	26.15/0.7459	24.42/0.6947	23.49/0.6416
Average	26.58/0.8103	24.72/0.6439	26.38/0.7905	25.39/0.7188	26.08/0.7868	24.06/0.7286	22.91/0.6566

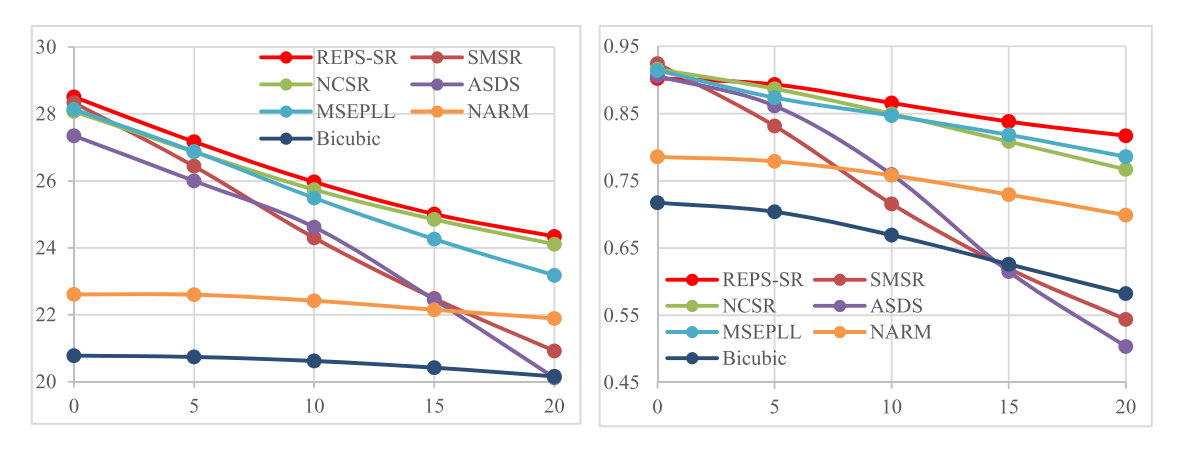


Fig. 9. PSNR and SSIM results of the proposed method and other state-of-the-art SR methods on "Butterfly" image with gradually increasing noise levels.

situations when λ_2 is fixed. From the visual comparison, the reconstructed image of the adaptively smoothing-aware scheme is smoother and cleaner than that of a fixed parameter. Such a situation indicates that for different noise levels, it is necessary to adaptively determine a variable smoothing-aware factor λ_2 . Therefore, we propose to use a function to fit the relationship between the smoothing-aware factor and the noise level of LR image. The factor can be adaptively determined

without manual interference. Experimental results indicate the effectiveness of this adaptive smoothing-aware scheme.

D. Performance on Real-Life Noisy Images

In this subsection, the performance of the proposed method and the comparison methods on real-life noisy images is provided. The noisy images are obtained from LIVE In the

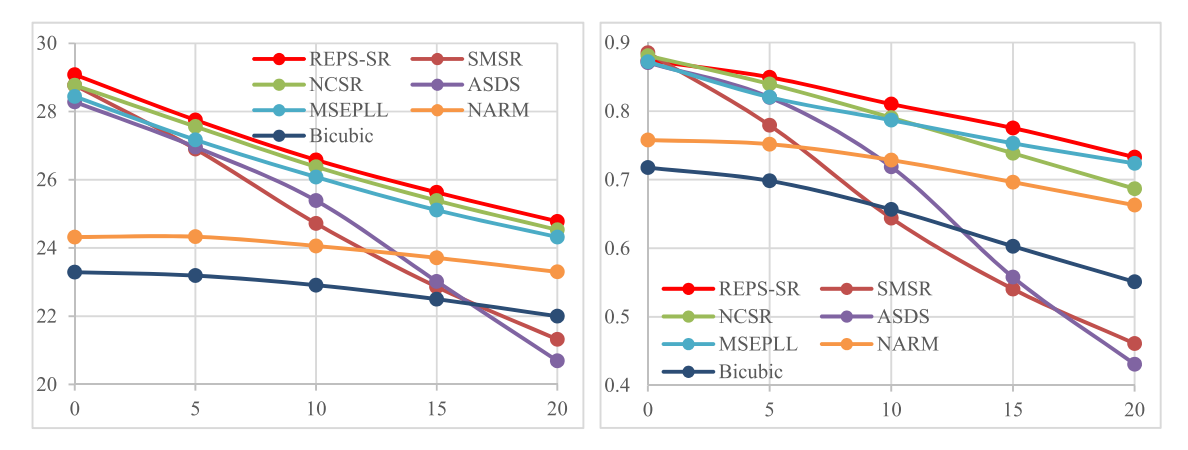


Fig. 10. Average PSNR and SSIM results of the proposed method and other state-of-the-art SR methods on twelve test images with gradually increasing noise levels.

 $TABLE\ V$ PSNR (dB)/SSIM Results on the Reconstruction of HR Images With a Scale Factor of 3

λ_2	adaptive smoothing-aware factor λ_2				$\lambda_2 = 0.3$			$\lambda_2 = 0.8$		
noise level	$\sigma=0$	<i>σ</i> =5	σ =10	$\sigma=0$	<i>σ</i> =5	σ =10	$\sigma=0$	<i>σ</i> =5	<i>σ</i> =10	
Flower	29.59/0.8530	28.26/0.8063	27.10/0.7564	29.40 /0.8287	28.26/0.8060	27.04/0.7483	28.70/0.7773	28.27/0.8061	27.08/0.7551	
Hat	31.39/0.8631	30.19/0.8352	29.14/0.8066	31.11/0.8277	30.18/ 0.8354	28.98/0.7879	29.51/0.7241	30.21 /0.8354	29.13/0.8055	
Plants	34.10/0.9169	31.99/0.8652	30.49/0.8222	28.98/0.7879	31.95/ 0.8641	30.33/0.8095	32.78/0.8505	31.95/0.8644	30.48/0.8206	
Parrots	30.51/0.9077	29.57/0.8836	28.35/0.8567	30.16/0.8642	29.56/0.8832	28.26/0.8461	28.81/0.7751	29.57/0.8829	28.34/0.8559	

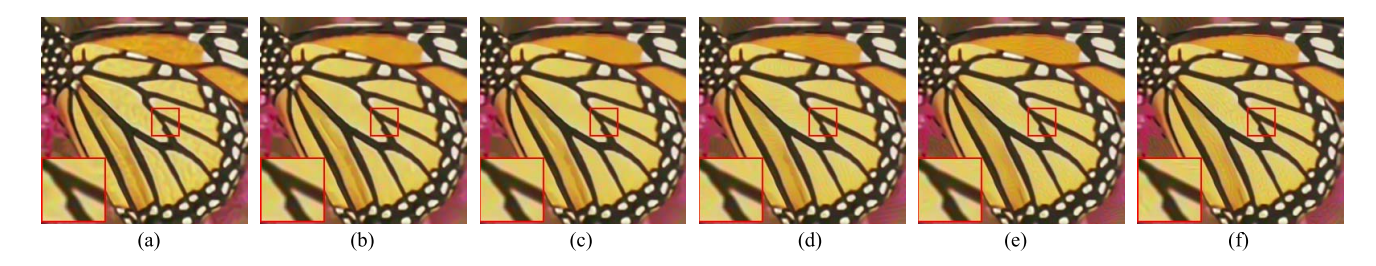


Fig. 11. The effects of λ_2 on the recovered HR images given the same input (scaling factor 3, noise level 10). (a) $\lambda_2=0$ (b) $\lambda_2=0.5$. (c) $\lambda_2=1.0$. (d) $\lambda_2=1.5$. (e) $\lambda_2=2.0$. (f) $\lambda_2=2.5$.

TABLE VI
AVERAGE RUNNING TIME OF DIFFERENT METHODS

Method	NARM	MSEPLL	ASDS	NCSR	SMSR	REPS-SR
Average Time	94.14s	327.24s	174.06s	191.05s	307.06s	200.47s

Wild Image Quality Challenge Database¹ in which the distortion type is unknown. The images with size of 500×500 are down-sampled by a scale factor of 3 and then used to generate HR images. The visual comparison samples are shown in Figs. 12 and 13, respectively. As shown in these figures, we can observe that the proposed REPS-SR method can preserve image edges well and the smooth regions are much cleaner than these from NCSR and ASDS methods. SMSR and NARM methods reconstruct the HR images with

¹LIVE In the Wild Image Quality Challenge Database. Online: http://live.ece.utexas.edu/research/ChallengeDB/index.html, 2015.

blur image edges and suffer from noise. Although MSEPLL method performs well on reconstructed image edges, the noise in smooth regions cannot be removed. Compared with these existing methods, the proposed method is more robust and can obtain consistently better performance on real-life noisy images.

E. Complexity Analysis

To evaluate the computational complexity of the proposed method, we conduct the comparison experiment for computational complexity of different methods on 10 images rescaled

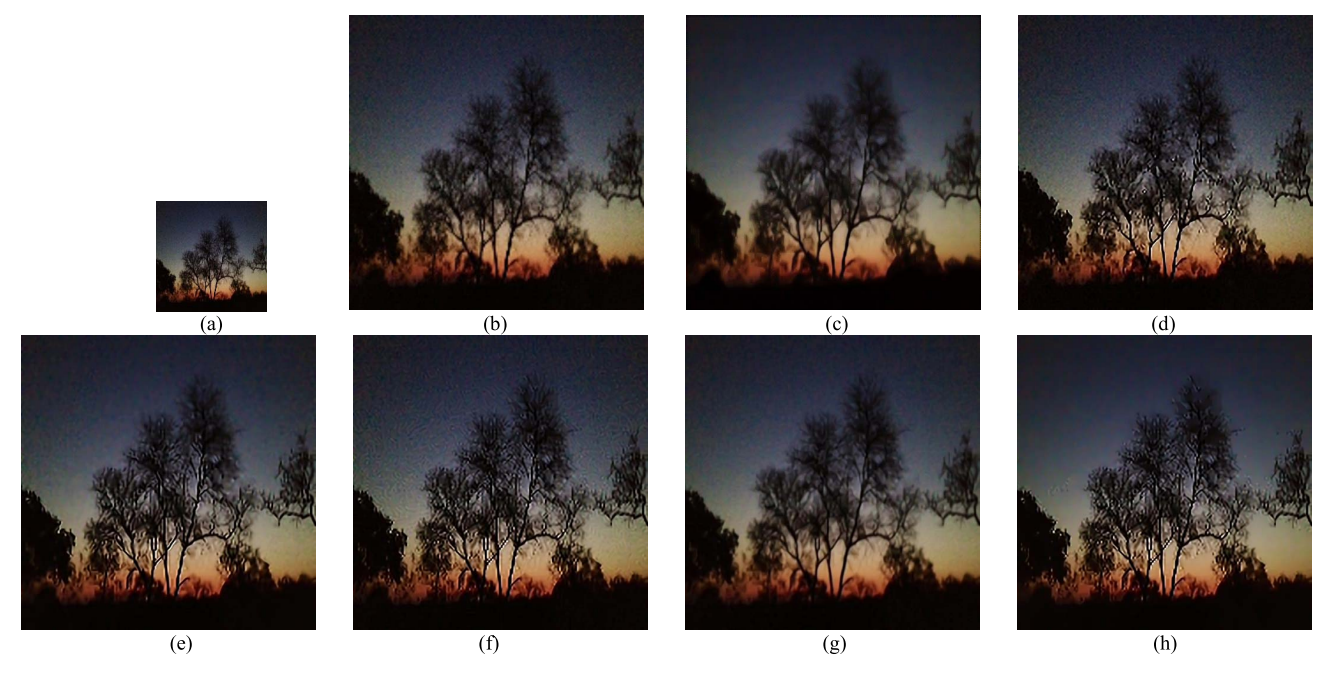


Fig. 12. Visual comparison samples of the proposed method and other state-of-the-art methods on real-life noisy image (number 1079 in the database) with a scale factor of 3. (a) LR. (b) Bicubic. (c) NARM. (d) MSEPLL. (e) ASDS. (f) NCSR. (g) SMSR. (h) REPS-SR.

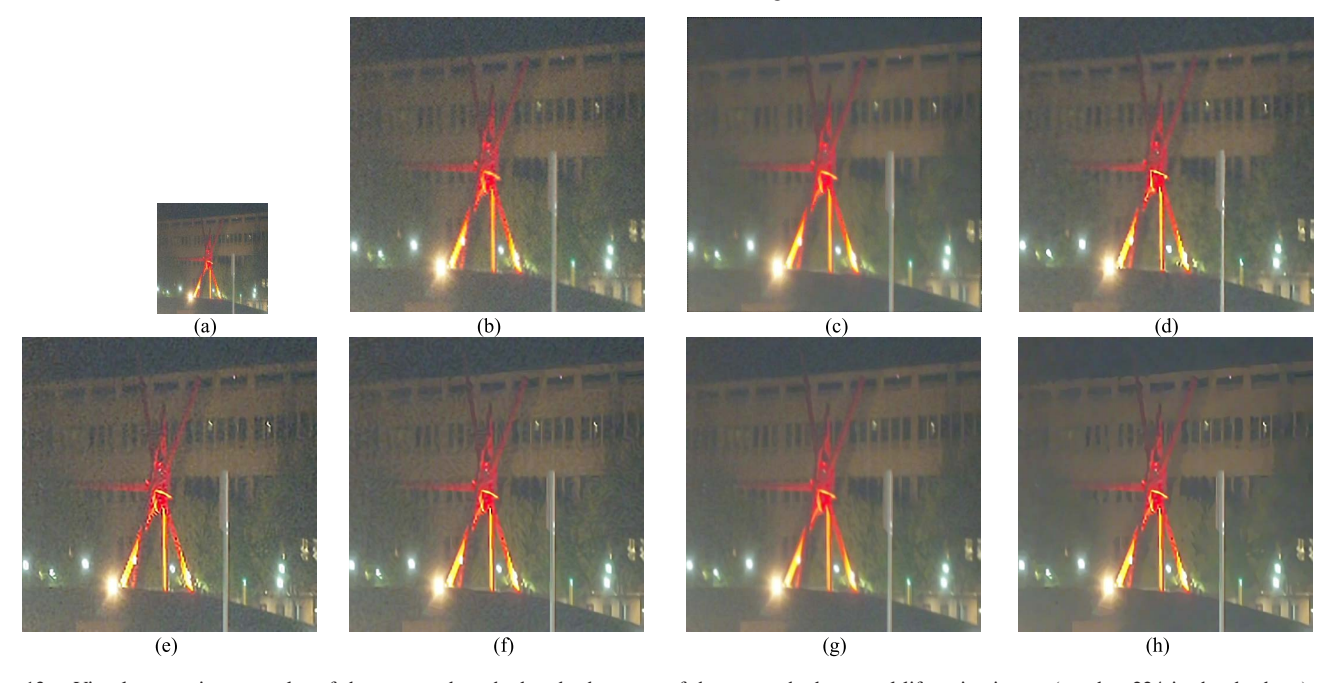


Fig. 13. Visual comparison samples of the proposed method and other state-of-the-art methods on real-life noisy image (number 224 in the database) with a scale factor of 3. (a) LR. (b) Bicubic. (c) NARM. (d) MSEPLL. (e) ASDS. (f) NCSR. (g) SMSR. (h) REPS-SR.

to 256×256 pixels on the $3 \times$ image enlargement task. We calculate the average running time of the proposed method and five representative methods for these test images using MATLAB 2014b on a computer with Intel(R) Core (TM) i7-6700HQ@2.60 GHz and 64-bit Windows 10 operating system. The running time of the compared methods are reported in Table VI. The proposed method takes an average time of 200.47s for a 256×256 image, while NCSR method takes an average time of 191.05s. The other sparse representation based methods (NARM, ASDS, and SMSR) take an average time of 94.14s, 174.06s, and 307.06s. The proposed method

improves SR performance at a cost of approximately equal running time compared with NCSR method. Note that, the proposed method is implemented by MATLAB, and the speed could be improved by implementing it in C++.

V. CONCLUSION

In this paper, we propose a novel robust single-image SR method. An EPS regularization term is designed to improve the SR performance. Image nonlocal self-similarity is incorporated into the proposed method to further improve SR performance both in objective and subjective evaluations. Extensive

experiments are conducted to explore the relationship between the added Gaussian noise level and the proposed smoothingaware factor. An adaptively determined the smoothing-aware factor scheme is designed by estimating the unknown noise level from the observed LR image. Experiments have demonstrated that the REPS-SR method is competitive with other leading SR methods when the noise level is zero and outperforms the state-of-the-art methods when larger noise levels are added, which indicates the robustness of the proposed method.

REFERENCES

- L. Yue, H. Shen, J. Li, Q. Yuanc, H. Zhang, and L. Zhang, "Image superresolution: The techniques, applications, and future," *Signal Process.*, vol. 128, pp. 389–408, Nov. 2016.
- [2] H. Wang, X. Gao, K. Zhang, and J. Li, "Single-image super-resolution using active-sampling Gaussian process regression," *IEEE Trans. Image Process.*, vol. 25, no. 2, pp. 935–948, Feb. 2016.
- [3] Y. Zhang, J. Liu, W. Yang, and Z. Guo, "Image super-resolution based on structure-modulated sparse representation," *IEEE Trans. Hum.-Mach. Syst.*, vol. 24, no. 9, pp. 2797–2810, Sep. 2015.
- [4] S. C. Park, M. K. Park, and M. G. Kang, "Super-resolution image reconstruction: A technical overview," *IEEE Signal Process. Mag.*, vol. 20, no. 3, pp. 21–36, May 2003.
- [5] Y. Li, Y. Wang, Y. Li, L. Jiao, X. Zhang, and R. Stolkin, "Single image super-resolution reconstruction based on genetic algorithm and regularization prior model," *Inf. Sci.*, vol. 372, pp. 196–207, Dec. 2016.
- [6] R. Y. Tsai and T. S. Huang, "Multiframe image restoration and registration," Adv. Comput. Vis. Image Process., vol. 1, no. 2, pp. 317–339, 1984.
- [7] C. Ren, X. He, and T. Q. Nguyen, "Single image super-resolution via adaptive high-dimensional non-local total variation and adaptive geometric feature," *IEEE Trans. Image Process.*, vol. 26, no. 1, pp. 90–106, Jan. 2017.
- [8] J. Jiang, X. Ma, C. Chen, T. Lu, Z. Wang, and J. Ma, "Single image super-resolution via locally regularized anchored neighborhood regression and nonlocal means," *IEEE Trans. Multimedia*, vol. 19, no. 1, pp. 15–26, Jan. 2017.
- [9] L. J. Deng, W. Guo, and T.-Z. Huang, "Single image super-resolution by approximated Heaviside functions," *Inf. Sci.*, vol. 348, pp. 107–123, Jun. 2016.
- [10] C. Dong, C. C. Loy, K. He, and X. Tang, "Image super-resolution using deep convolutional networks," *IEEE Trans. Pattern Anal. Mach. Intell.*, vol. 38, no. 2, pp. 295–307, Feb. 2015.
- [11] S. Farsiu, M. D. Robinson, M. Elad, and P. Milanfar, "Fast and robust multiframe super resolution," *IEEE Trans. Image Process.*, vol. 13, no. 10, pp. 1327–1344, Oct. 2004.
- [12] D. Capel and A. Zisserman, "Super-resolution from multiple views using learnt image models," in *Proc. IEEE Conf. Comput. Vis. Pattern Recognit.*, vol. 2. Dec. 2001, pp. 627–634.
- [13] Q. Yuan, L. Zhang, and H. Shen, "Multiframe super-resolution employing a spatially weighted total variation model," *IEEE Trans. Circuits Syst. Video Technol.*, vol. 22, no. 3, pp. 379–392, Mar. 2012.
- [14] A. W. M. van Eekeren, K. Schutte, and L. J. van Vliet, "Multiframe super-resolution reconstruction of small moving objects," *IEEE Trans. Image Process.*, vol. 19, no. 11, pp. 2901–2912, Nov. 2010.
- [15] K. I. Kim and Y. Kwon, "Single-image super-resolution using sparse regression and natural image prior," *IEEE Trans. Pattern Anal. Mach. Intell.*, vol. 32, no. 6, pp. 1127–1133, Jun. 2010.
- [16] Z. Zhu, F. Guo, H. Yu, and C. Chen, "Fast single image superresolution via self-example learning and sparse representation," *IEEE Trans. Multimedia*, vol. 16, no. 8, pp. 2178–2190, Dec. 2014.
- [17] N. Qi, Y. Shi, X. Sun, W. Ding, and B. Yin, "Single image super-resolution via 2D sparse representation," in *Proc. IEEE Int. Conf. Multimedia Expo*, Jun./Jul. 2015, pp. 1–6.
- [18] S. Rhee and M. G. Kang, "Discrete cosine transform based regularized high-resolution image reconstruction algorithm," *Opt. Eng.*, vol. 38, no. 8, pp. 1348–1356, 1999.
- [19] H. Demirel, S. Izadpanahi, and G. Anbarjafari, "Improved motion-based localized super resolution technique using discrete wavelet transform for low resolution video enhancement," in *Proc. Eur. Signal Process. Conf.*, Aug. 2009, pp. 1097–1101.

- [20] M. S. Alam, J. G. Bognar, R. C. Hardie, and B. J. Yasuda, "Infrared image registration and high-resolution reconstruction using multiple translationally shifted aliased video frames," *IEEE Trans. Instrum. Meas.*, vol. 49, no. 5, pp. 915–923, Oct. 2002.
- [21] B. Wan, L. Meng, D. Ming, H. Qi, Y. Hu, and K. D. K. Luk, "Video image super-resolution restoration based on iterative back-projection algorithm," in *Proc. IEEE Int. Conf. Comput. Intell. Meas. Syst. Appl.*, May 2009, pp. 46–49.
- [22] H. Stark and P. Oskoui, "High-resolution image recovery from imageplane arrays, using convex projections," J. Opt. Soc. Amer. A, Opt. Image Sci., vol. 6, no. 11, pp. 1715–1726, 1989.
- [23] K. Zhang, X. Gao, D. Tao, and X. Li, "Single image super-resolution with non-local means and steering kernel regression," *IEEE Trans. Image Process.*, vol. 21, no. 11, pp. 4544–4556, Nov. 2012.
- [24] T. Sigitani, Y. Iiguni, and H. Maeda, "Image interpolation for progressive transmission by using radial basis function networks," *IEEE Trans. Neural Netw.*, vol. 10, no. 2, pp. 381–390, Mar. 1999.
- [25] X. Li and M. T. Orchard, "New edge-directed interpolation," IEEE Trans. Image Process., vol. 10, no. 10, pp. 1521–1527, Oct. 2001.
- [26] L. Zhang and X. Wu, "An edge-guided image interpolation algorithm via directional filtering and data fusion," *IEEE Trans. Image Process.*, vol. 15, no. 8, pp. 2226–2238, Aug. 2006.
- [27] M. Protter, M. Elad, H. Takeda, and P. Milanfar, "Generalizing the nonlocal-means to super-resolution reconstruction," *IEEE Trans. Image Process.*, vol. 18, no. 1, pp. 36–51, Jan. 2009.
- [28] J. Sun, Z. Xu, and H.-Y. Shum, "Image super-resolution using gradient profile prior," in *Proc. IEEE Conf. Comput. Vis. Pattern Recognit.*, Jun. 2008, pp. 1–8.
- [29] K. Zhang, X. Gao, X. Li, and D. Tao, "Partially supervised neighbor embedding for example-based image super-resolution," *IEEE J. Sel. Topics Signal Process.*, vol. 5, no. 2, pp. 230–239, Apr. 2011.
- [30] R. Timofte, V. De, and L. Van Gool, "Anchored neighborhood regression for fast example-based super-resolution," in *Proc. IEEE Int. Conf. Comput. Vis.*, Dec. 2013, pp. 1920–1927.
- [31] L. He, H. Qi, and R. Zaretzki, "Beta process joint dictionary learning for coupled feature spaces with application to single image superresolution," in *Proc. IEEE Conf. Comput. Vis. Pattern Recognit.*, Portland, OR, USA, Jun. 2013, pp. 345–352.
- [32] X. Li, H. He, R. Wang, and D. Tao, "Single image superresolution via directional group sparsity and directional features," *IEEE Trans. Image Process.*, vol. 24, no. 9, pp. 2874–2888, Sep. 2015.
- [33] Y.-W. Tai, S. Liu, M. S. Brown, and S. Lin, "Super resolution using edge prior and single image detail synthesis," in *Proc. IEEE Conf. Comput. Vis. Pattern Recognit.*, Jun. 2010, pp. 2400–2407.
- [34] J. Sun, J. Sun, Z. Xu, and H.-Y. Shum, "Gradient profile prior and its applications in image super-resolution and enhancement," *IEEE Trans. Image Process.*, vol. 20, no. 6, pp. 1529–1542, Jun. 2011.
- [35] J. Mairal, F. Bach, J. Ponce, G. Sapiro, and A. Zisserman, "Non-local sparse models for image restoration," in *Proc. Int. Conf. Comput. Vis.*, 2009, pp. 2272–2279.
- [36] J. Yang, J. Wright, T. S. Huang, and Y. Ma, "Image super-resolution via sparse representation," *IEEE Trans. Image Process.*, vol. 19, no. 11, pp. 2861–2873, Nov. 2010.
- [37] W. Dong, L. Zhang, G. Shi, and X. Wu, "Image deblurring and super-resolution by adaptive sparse domain selection and adaptive regularization," *IEEE Trans. Image Process.*, vol. 20, no. 7, pp. 1838–1857, Jul. 2011.
- [38] T. Peleg and M. Elad, "A statistical prediction model based on sparse representations for single image super-resolution," *IEEE Trans. Image Process.*, vol. 23, no. 6, pp. 2569–2582, Jun. 2014.
- [39] Z. Wang, D. Liu, J. Yang, W. Han, and T. Huang, "Deep networks for image super-resolution with sparse prior," in *Proc. IEEE Int. Conf. Comput. Vis.*, Dec. 2015, pp. 370–378.
- [40] V. Papyan and M. Elad, "Multi-scale patch-based image restoration," IEEE Trans. Image Process., vol. 25, no. 1, pp. 249–261, Jan. 2016.
- [41] W. Dong, L. Zhang, R. Lukac, and G. Shi, "Sparse representation based image interpolation with nonlocal autoregressive modeling," *IEEE Trans. Image Process.*, vol. 22, no. 4, pp. 1382–1394, Apr. 2013.
- [42] R. Zeyde, M. Elad, and M. Protter, "On single image scale-up using sparse-representations," in *Proc. 7th Int. Conf. Curves Surfaces*, 2010, pp. 711–730.
- [43] R. Rubinstein, T. Peleg, and M. Elad, "Analysis K-SVD: A dictionary-learning algorithm for the analysis sparse model," *IEEE Trans. Signal Process.*, vol. 61, no. 3, pp. 661–677, Feb. 2013.

- [44] W. Dong, L. Zhang, G. Shi, and X. Li, "Nonlocally centralized sparse representation for image restoration," *IEEE Trans. Image Process.*, vol. 22, no. 4, pp. 1620–1630, Apr. 2013.
- [45] F. Kou, W. Chen, C. Wen, and Z. Li, "Gradient domain guided image filtering," *IEEE Trans. Image Process.*, vol. 24, no. 11, pp. 4528–4539, Nov. 2015.
- [46] I. Daubechies, M. Defrise, and C. De Mol, "An iterative thresholding algorithm for linear inverse problems with a sparsity constraint," *Commun. Pure Appl. Math.*, vol. 57, no. 11, pp. 1413–1457, Nov. 2004.
- [47] S. Yang, M. Wang, Y. Chen, and Y. Sun, "Single-image super-resolution reconstruction via learned geometric dictionaries and clustered sparse coding," *IEEE Trans. Image Process.*, vol. 21, no. 9, pp. 4016–4028, Sep. 2012.
- [48] C. He, C. Hu, W. Zhang, and B. Shi, "A fast adaptive parameter estimation for total variation image restoration," *IEEE Trans. Image Process.*, vol. 23, no. 12, pp. 4954–4967, Dec. 2014.
- [49] X. Liu, M. Tanaka, and M. Okutomi, "Single-image noise level estimation for blind denoising," *IEEE Trans. Image Process.*, vol. 22, no. 12, pp. 5226–5237, Dec. 2013.
- [50] X. Liu, M. Tanaka, and M. Okutomi, "Noise level estimation using weak textured patches of a single noisy image," in *Proc. 19th IEEE Int. Conf. Image Process.*, Orlando, FL, USA, 2012, pp. 665–668.
- [51] Z. Wang, A. C. Bovik, H. R. Sheikh, and E. P. Simoncelli, "Image quality assessment: From error visibility to structural similarity," *IEEE Trans. Image Process.*, vol. 13, no. 4, pp. 600–612, Apr. 2004.



Shuying Huang (M'14) received the Ph.D. degree in computer application technology from the Ocean University of China, Qingdao, China, in 2013. She is currently an Associate Professor with the School of Software and Communication Engineering, Jiangxi University of Finance and Economics, Nanchang, China. Her current research interests include image and signal processing, and pattern recognition.



Jun Sun received the B.S. degree in communication engineering from Henan Polytechnic University, Jiaozuo, China, in 2015. He is currently pursuing the M.S. degree in electronic and communication engineering with the Jiangxi University of Finance and Economics, Nanchang, China. His current research interests include image super resolution, sparse representation, and image processing.



Yong Yang (M'13–SM'16) received the Ph.D. degree from Xi'an Jiaotong University, Xi'an, China, in 2005. From 2009 to 2010, he was a Post-Doctoral Research Fellow with Chonbuk National University, Jeonju, South Korea. He is currently a Full Professor and the Vice Dean with the School of Information Technology, Jiangxi University of Finance and Economics, Nanchang, China. His current research interests include image fusion and super resolution, image processing and analysis, and pattern recognition. He received the title of Jiangxi Province Young

Scientist in 2012, and was selected as the Jiangxi Province Thousand and Ten Thousand Talent in 2015. He is an Associate Editor of the IEEE Access and the Editor of the KSII Transactions on Internet and Information Systems.



Yuming Fang (M'13) received the B.E. degree from Sichuan University, Chengdu, China, the M.S. degree from the Beijing University of Technology, Beijing, China, and the Ph.D. degree from Nanyang Technological University, Singapore. He is currently a Professor with the School of Information Technology, Jiangxi University of Finance and Economics, Nanchang, China. He has authored and co-authored over 90 academic papers in international journals and conferences in the areas of multimedia processing. His research interests include visual attention

modeling, visual quality assessment, image retargeting, computer vision, and 3D image/video processing. He serves as an Associate Editor of the IEEE ACCESS and is on the Editorial Board of *Signal Processing: Image Communication*.



medical engineering from Xi'an Jiaotong University, Xi'an, China, in 2005. From 2007 to 2011, he was a Post-Doctoral Researcher with the Center for Mind/Brain Sciences, University of Trento, Italy. From 2013 to 2014, he was a Research Fellow with Mclean Hospital, Harvard Medical School, Boston, MA, USA. Since 2017, he has been a Professor with the College of Biomedical Engineering, South-Central University for Nationalities, Wuhan, China. His current research interests include multimodal

Pan Lin (M'16) received the Ph.D. degree in bio-

His current research interests include multimodal MRI imaging, medical image processing, image processing, and pattern recognition.



Yue Que received the B.S. degree in educational technology from Nanchang Hangkong University, Nanchang, China, in 2013. He is currently pursuing the M.S. degree in computer technology with the Jiangxi University of Finance and Economics, Nanchang, China. His current research interests include image fusion, fuzzy pattern recognition, and image processing.